Available online at www.sciencedirect.com

ScienceDirect

Procedia CIRP 74 (2018) 654–658

www.elsevier.com/locate/procedia

10th CIRP Conference on Photonic Technologies [LANE 2018]

Laser processing quality monitoring by combining acoustic emission and machine learning: a high-speed X-ray imaging approach

K. Wasmer[a*], T. Le-Quang[a], B. Meylan[a], F. Vakili-Farahani[a], M.P. Olbinado[b], A. Rack[b], S.A. Shevchik[a]

[a]*Swiss Federal Laboratories for Materials Science and Technology (Empa), Laboratory for Advanced Materials Processing (LAMP), Switzerland*
[b]*ESRF—The European Synchrotron, CS40220, F-38043 Grenoble, France*

* Corresponding author. Tel.: +41-58-765-6271 ; fax: +41-58-765-6990. *E-mail address: kilian.wasmer@empa.ch*

Abstract

In situ and real-time monitoring of laser processes are very challenging due to complex dynamics of the laser-matter interactions. Acoustic emission (AE) technique is often used as non-destructive monitoring of many kinds of processes. However, acoustic emission is not industrialized for laser processing for two reasons. First, the signals are too sensitive to the environmental noises. Second, a correlation of the acoustic emission signal with the real events is very difficult to realize despite being of utmost importance. To overcome these difficulties, we combined fast hard X-ray imaging with acoustic sensors and state-of-the-art machine learning.

Peer-review under responsibility of the Bayerisches Laserzentrum GmbH.

Keywords: "Laser welding, in situ and real-time, monitoring, High speed X-ray, acoustic, machine learning"

1. Introdution

Laser processing is a demanding technology which is involved in a growing number of applications, including: welding, cutting, drilling, polishing, additive manufacturing and many others. Despite lasers' advantages, laser-matter interaction is a highly complex dynamic process with short life-time events, making its monitoring challenging [1].

Acoustic emission (AE) is known to be very robust in detecting various physical phenomena; with affordable hardware realizations possible. Hence, AE is widely used for process monitoring [2]. Since, AE is able to detect a broad spectrum of events in a wide range of time-scales; it is a promising solution to monitor laser processes. Some innovative approaches combine AE with state-of-the-art machine learning techniques for in situ and real-time quality monitoring of laser processes such as welding and additive manufacturing [3,4]. The major challenge is to correlate the AE signals with the real events that occur within a dense and non-transparent material. One method for making such correlations is, in most cases, performed post mortem via analysis of cross-sections. Unfortunately, the random fluctuations in the AE signals makes this highly demanding from a signal processing point of view.

To overcome this difficulty, several series of laser welding experiments were conducted at the European Synchrotron Radiation Facility (ESRF, Grenoble, France) using high-speed X-ray radiography combined with AE measurements. This allowed us to visualize the complete dynamics of the laser-material interactions and simultaneously acquire the corresponding AE signals. The entire laser welding process was divided into four categories: *conduction welding*, *stable keyhole*, *unstable keyhole* and *spatter*. The collected AE signals were synchronized with the video sequences and labeled accordingly. The correlation of the AE signals with the four aforementioned defined categories were made using gradient boost (GB), a state-of-the-art machine learning method, with two learners: i) classifications and regression trees CART, and ii) trees based on independent component analysis (ICA).

Peer-review under responsibility of the Bayerisches Laserzentrum GmbH.
10.1016/j.procir.2018.08.054

2. Experimental method

2.1. Experimental setup, data acquisition and categorization

Laser welding experiments were carried out using a single-mode fiber laser source StarFiber 150 P (Fiber laser–StarFiber 150 P/300 P) with a 1070 nm wavelength and a Gaussian shape beam. A focal lens of 170 mm provided a diameter spot size of about 30 µm at the focal point ($2w_0$).

The acoustic signals were recorded using a piezo acoustic sensor Pico (Physical Acoustics, USA). The digitalization and data storage was provided by a data acquisition unit and software from Vallen (Vallen Gmbh, Germany). The data collection was performed with a sampling rate of 10 MHz. The piezo acoustic sensor was attached to the sample holder at the same position throughout all experiments.

An aluminum-magnesium alloy was chosen for its relative low *Z*-number. The samples had dimensions 50 x 20 x 2 mm^3.

The high-speed X-ray imaging was made at the beamline ID19 of the ESRF using the synchrotron X-ray source in polychromatic mode: high photon flux that could be exploited for X-ray radiography up to millions frames per second (fps) rates [5]. X-ray phase contrast imaging by free-space propagation was mounted to enhance the contrast between material interfaces. A U-13 type undulator (single harmonic) at minimum gap of 11.1 mm was used. A diamond filter and an aluminium filter of 1.4 mm thickness each were installed to suppress lower photon energies. The pink beam mean energy was 26.3 keV. The radiography of the laser welding process was recorded by an indirect X-ray detector composed of a 250 µm-thick Ce-doped $Lu_3Al_5O_{12}$ scintillator, lens-coupled to a high-speed camera (pco.dimax; PCO, Germany) at a 90° angle using a mirror. The range of recording frame rates during the experiments was 28 000 to 36 000 fps. The effective pixel size of the X-ray image detector was 11 µm.

In this work and based on the X-ray imaging, four categories were defined: 1) *conduction welding*, 2) *stable keyhole*, 3) *unstable keyhole*, 4) *spatter*. A typical image of the categories 1 to 4 is shown in Fig. 1. More details on the experimental setup are given in [6].

2.2. Signals preprocessing

Wavelet packet transform (WPT) [7], which is a special technique for analyzing non-stationary signals, was applied to the acquired AE signals. The WPT result is the splitting of the time-frequency space into a finite number of the narrow bands [7]. In this study, the relative energies of the extracted frequency bands were computed in compliance with the work of Saeidi *et al.* [8] . The signal representation provided a discretized and sparse representation of the signal flow. It allowed capturing the local particularities with a lower noise levels due to the wavelets properties [7] and, at the same time, reduced the amount of the input data for the next processing stage [8]. More details on wavelets techniques related to real-life data are given in the review of Mallat [7].

In this work, the labeled acoustic signals were cut into separate patterns having each a duration of 1.2 ms. The narrow frequency bands were extracted for each such pattern with WPT. Thereafter, only the relative energies of the frequency bands from the third to the seventh decomposition levels were selected. Doing so, it excluded the presence of noise, where the main sources came from the experimental setup and surrounding environment. This resulted in the substitution of each acoustic pattern by 248 values of the relative energies of the frequency bands that were further analyzed in a machine learning framework.

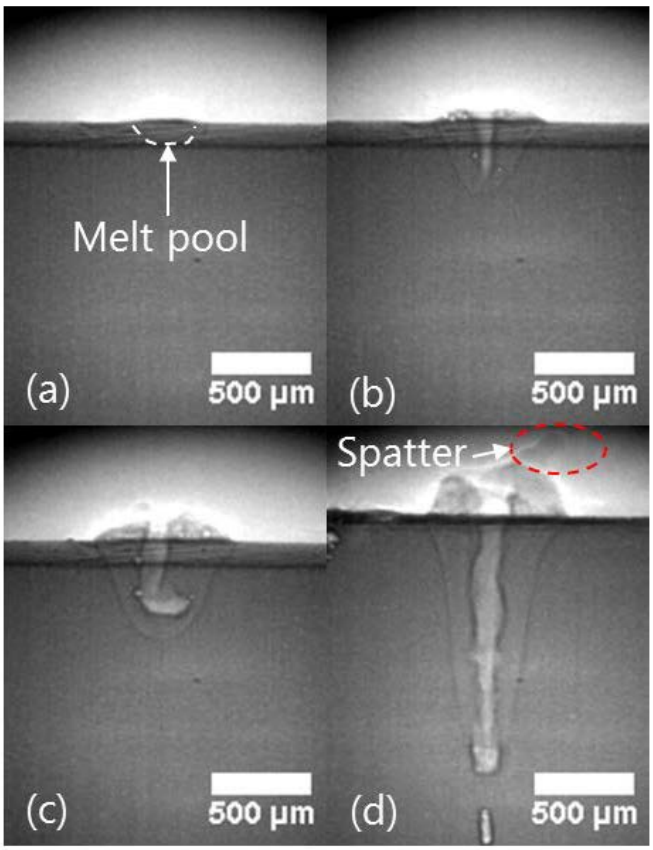

Fig. 1. Real-time X-ray images of (1) *conduction welding*, (2) *stable keyhole*, (3) *unstable keyhole*, and (4) *spatter*.

2.3. Gradient boost

The analysis of the acquired AE data (i.e. the recognition of a predefined number of momentary events in a continuous signal flow) is performed with machine learning (ML) classification. To perform this task, a gradient boost (GB) [9] was applied to the pre-processed signal. GB is an extension of a more general boosting technique [10], which is a branch of ML that employs a number of weak classifiers to build a strong one [9,10]. We chose the boosting technique for its natural advantages when analyzing real-life data; namely: insensitivity to outliers, easy scalability and resolution of the non-linear cases due to its hierarchical architecture [10]. GB enhances the boosting by involving a specialized optimization, which introduces weak learners with a gradient descent procedure, as a way to minimize some global loss [9]. An additional flexibility of boosting, and in particular for GB, is in the introduction of a specific loss functions and optimizations suiting at best the problem without changing the

general framework [10]. We exploited fully the advantages of this algorithm and the details are described below.

In GB, the training set includes a number of pairs $z = \{X_i, Y_i\}$, where X_i is an array with the attribute values (the relative energies of the narrow frequency bands extracted with DPT) and Y_i is a specific classifier response to each pre-defined momentary laser welding event. The estimation of the classifier mapping rule $Y_i = F(X_i)$ is a subject for the training procedure. As already mentioned, the solution of the GB problem is in minimizing the following functional [10,11]:

$$C(F) = {}^{1}/_{n} \sum_n L(F(X_i), Y_i) \quad (1)$$

where $L()$ is a so-called loss function. We chose the loss function among the common collection, used for classification tasks that includes logistic, hinge and exponential functions [10,11]. Those are suitable for binary cases $\{Y = \pm 1\}$ and fitted this study, where one against all strategy is applied to resolve multiple categories. None of the aforementioned loss functions gave advantages in the classification during tests. In Table 3, the results are presented for logistic loss function: $L = ln(1\text{-}exp^{-YF(X)})$. The mapping rule $F()$ is a linear combination of a number of classifiers: $F(X) = \sum_n f_i(X)$. We used binary decision trees where $f()$ was a splitting rule in the tree terminal nodes [12]. The solution for Eq. (1) can be achieved using either the approximate identities [11,13] or the mean least squares approximations [11,14]. Both approaches had equal efficiency in solving Eq. (1) [11]. In this investigation, the mean least squares approximation [14] was taken without any prior preference. In all aforementioned techniques, the gradient descent for Eq. (1) is carried out over the function space, each iteration introducing a new f with a specified direction that reduces the loss L in Eq. (1) [11]. The pseudo scheme of the algorithm is given in Table 1 [14].

Table 1. Minimization of the functional through gradient descent [11]

For each m from the pre-defined number of iterations M:	
Step 1	Computation of $\nabla C = -\partial\, C(Y_i, F(X_i))/\partial\, F(X_i)$, where $F(X_i) = F_{m-1}(X_i)$ is taken from the previous iteration step
Step 2	Update the mapping rule as: $F_m(X) = F_{m-1}(X) + \lambda_m f_m(X)$, and at the same time, computing the individual magnitude step λ_m and the directions of f_m that maximizes $-\nabla C$
Step 3	Assign $m\text{-}1$ to m and repeat Step 1

The search of the directions for each individual f that maximizes -∇C (see Table 1, Step 2) is a separate sub-task of the problem. While several strategies already exist [11,12,15], our search of the most optimal one was done to fit best the data from our laser welding experiments and it was the objective of an additional sub-study. The aim was to check the sensitivity of the classification trees on the final classification performance within existing GB methodology [11,13,14].

The collected data could be uploaded at once into the memory which included a limited number of signals. This important aspect implied that the structure of the entire data could be analyzed before its processing, avoiding a blind search during hierarchical splits in f as described. This aspect excluded the need to approximate the solutions which requires specific methods and is employed for large datasets [15]. Taking advantage of this, we made a pre-processing to guide the splits f during the optimization process (see Table 1).

The splits f of the input data into a number of subsets using the terminal nodes and the features were obtained from the tree leafs [12]: $f = \sum_k \lambda_i 1_A$, where λ and A are the weights (normalized or not) and split partitions, respectively, k is the tree depth [13,14]. The estimation of the optimal split is not a trivial task [16] and two strategies were investigated, which uses discrete and continuous attribute values. This implies that, in the context of the wavelet spectrograms, those two strategies break or keep the order of the narrow frequency bands in the time domain and so are of interest for the investigation. For the discrete case, the classical decision trees CART [12] were taken. In CART, the optimal splits were estimated through an exhaustive search among all possible combinations minimizing some impurity (Gini) criterion [12]. The second strategy considered was the independent component analysis (ICA) [17] for decision tree induction; in particular, the tree architecture developed by Pajunen *et al.* [18]. ICA has also the advantage of being able to recover the data structure independently from the labels [18], which is not a case in classical approaches [12,16]. This may result in an efficient unsupervised training but this was out of the scope of this study. ICA assumes that the observed data is a mix of some unobserved components, expressed by a statistical model [17]: $X = A\boldsymbol{s} + \varepsilon$, where ε is the mean-zero Gaussian noise. The goals of ICA were to recover the mixing law A and to extract the components $\boldsymbol{s}$. In the classical approach used, the solution is in minimization of the mutual information [17]:

$$I = \log|A| + \sum H(s_i) + H(X) \quad (2)$$

where the entropy H characterizes the structure of the data [17]. In ICA, the data with non-Gaussian distribution possesses more structure than the one with a Gaussian distribution. The de-mixing law W is an inverse of A and provides a recovery of the independent components [17]:

$$s' = W^T X \quad (3)$$

where s' is the approximate of s. In the case of the binary decision trees, the optimal direction of f can be identified from Eq. (3) as a choice of a single element from W *(e.g.* a split with the maximum non-Gaussianity) [18]. The solution for W involves the expectation minimization as proposed by Pajunen *et al.* [18] and the pseudo scheme is given in Table 2.

The ICA based trees included the information gain stopping rule as proposed by Quinlan [19]. Its computation was carried out using the entropy, evaluated during the ICA procedure for each subset, leading to the computations in a single thread flow.

Table 2. Minimization of the functional through gradient descent [11]

For each *n* variables:	
Step 1	Estimate mean for a subset X_n ɔ X and make zero mean transformations [17]: $X_0 = X_n - E\{X_n\}$
Step 2	Partition into to sub-sets X_{n1} and X_{n2} using: $W^T X_n > 0$ or $W^T X_n < 0$
Step 3	Find W from Eq. 3 using ICA
Step 4	Repeat Step 1for the two subsets X_{n1} and X_{n2}

Our technical developments were programmed in Microsoft Visual Studio 2017 in language - C#. We used and modified the code from the library CSharpLearning.NET [20]. The tests were made using a PC with i5 processor and 8 GB RAM. The processing time for pre-processing and classification of a single acoustic pattern was around 30 msec. This time is sufficient for an in situ and real-time process monitoring without specialized computational hardware.

2.4. Tests

The entire dataset had a total of 1'200 acoustic patterns that were distributed between the four welding categories according to: *conduction welding* – 300 patterns, *stable keyhole* – 300, *unstable keyhole* – 500, and *spatter* – 100. The evaluation of the classification strategy of the laser welding monitoring was made by dividing the dataset into two different sub-sets: one for training and one for testing. The two sub-sets had no common signals, which is exactly the situation encountered during operation in real-time conditions.

3. Results and discussion

The classification results are given in Table 3. In this table, the number in bold are obtained from GB [14] with ICA [18] whereas the ones in bracket are from GB [14] with the decision trees specified in CART [12]. The classification accuracies in the table are defined as the number of true positives divided by the total number of tests for each category. These values are given in the diagonal cells of the table (grey cells). The classification errors are computed as the number of the true negatives divided by the total number of the tests for each category. The corresponding values are filled in non-diagonal row cells. For the category *conduction*, the classification accuracy for ICA is as high as 95%. The misclassifications are with the categories *stable keyhole* and *unstable keyhole*, with errors of 3% and 2 %, respectively.

Based on Table 3, five observations can be made. First, the classification accuracy ranges between 74 and 95%. This demonstrates that our approach is a very promising technology for in situ and real-time monitoring of laser welding processes. Then, the classification accuracy decreases as the welding penetration increases (see grey cells). Third, GB with ICA has slightly higher classification accuracies as compared to GB with CART. Forth, the training time was reduced by 58% from 6 min to 3.5 min, respectively, which is a key for real-life conditions. Finally, most misclassification is with the neighbor category. This is certainly due to the fact that there is not a sharp transition between the categories.

Table 3. Classification results for the laser welding process monitoring. In bolt, the results obtained from gradient boost [14] with ICA [18] and in bracket using gradient boost [14] with CART [12].

Tests \ Ground truth	1	2	3	4
1- *conduction welding*	**95** (94)	**3** (3)	**2** (3)	**0** (0)
2 - *stable keyhole*	**3** (7)	**89** (85)	**8** (8)	**0** (0)
3 - *unstable keyhole*	**0** (2)	**8** (3)	**84** (89)	**8** (6)
4 - *spatter*	**3** (6)	**8** (8)	**11** (12)	**78** (74)

4. Conclusions

In this contribution, we combined high-speed X-Ray imaging, acoustic sensors and machine learning for in situ monitoring of laser welding. High-speed X-Ray imaging was used to correlate the acoustic emission (AE) signals with the real processing events. We defined four categories; *conduction welding*, *stable keyhole*, *unstable keyhole* and *spatter*. The classifications were made using gradient boost (GB) with both independent component analysis (ICA) and with CART, which are state-of-the-art machine learning (ML) techniques. The classifications accuracy ranged from 74 to 95%. This demonstrated that our innovative approach, combining AE and ML, is really promising for in situ and real-time monitoring of laser welding processes.

Acknowledgements

We would like to thanks Dr. Jörg Grenzer from Helmholtz-Zentrum Dresden-Rossendorf and Dr Christian Leinenbach from Empa for support during the beam time granted by the European Synchrotron Radiation Facility (MA-3477).

References

[1] You DY, Gao XD, Katayama S., Review of laser welding monitoring. Sci. Technol. Weld. Joining 2014;19(3):181-201, 10.1179/1362171813Y.0000000180.
[2] C. Grosse, M. Ohtsu, eds., Acoustic emission testing basics for research - applications in civil engineering, 1st ed., Springer, Berlin, Heidelberg, 2008, 10.1007/978-3-540-69972-9.
[3] Wasmer K, Kenel C, Leinenbach C, Shevchik SA, In situ and real-time monitoring of powder-bed AM combining acoustic emission and artificial intelligence. Proc. Additive Manufacturing in Products and Applications - AMPA2017, 10.1007/978-3-319-66866-6_20.
[4] Shevchik SA, Kenel C, Leinenbach C, Wasmer K, Acoustic emission for in situ quality monitoring in additive manufacturing using spectral convolutional neural networks. Ad. Man., 10.1016/j.addma.2017.11.012.
[5] Olbinado M.P., Just X., Gelet J.-L., Lhuissier P., Scheel M., Vagovic P., Sato T., Graceffa R., Schulz J., Mancuso A., Morse J., Rack A., MHz frame rate hard X-ray phase-contrast imaging using synchrotron radiation., Opt. Express. 2017;25:13857–13871, 10.1364/OE.25.013857
[6] Le Quang T, Shevchik SA, Meylan B, Olbinado MP, Rack A, Wasmer K, Why is in-situ quality control of laser keyhole welding a real challenge?, Procedia CIRP, 2018;xx:XXX-XXX.
[7] Mallat S, A wavelet tour of signal processing, 3rd Ed. Elsevier, 2009.
[8] Saeidi F, Shevchik SA, Wasmer K, Automatic detection of scuffing using acoustic emission, Trib. Int., 2016;94:112-117. 10.1016/j.triboint.2015.08.021.
[9] Friedman J.H., Stochastic Gradient Boosting, Comput. Stat. Data Anal. 2002;38 (4): 367–378, 10.1016/S0167-9473(01)00065-2.
[10] Hastie T, Tibshirani R, Friedman J, The elements of statistical learning: data mining, inference, and prediction. 2nd Ed. Springer, 2009.
[11] Biau G, Cadre B, Optimization by gradient boosting,

arxiv.org/abs/1707.05023v1 [math.ST] 17 Jul 2017.
[12] Breiman L, Friedman JH, Olshen RA, Stone CJ, Classification and Regression Trees. Chapman & Hall/CRC Press, Boca Raton, 1984.
[13] Mason L, Baxter J, Bartlett P, Frean M, Functional gradient techniques for combining hypotheses. Smola AJ, Bartlett PL, Schölkopf B, Schurmans D. eds, Cambridge, MA, TheMITPress, 2000:221–246.
[14] Friedman J.H., Greedy function approximation: A gradient boosting machine, Ann. Stat., 2001;29(5): 1189–1232, https://projecteuclid.org:443/euclid.aos/1013203451.
[15] Chen T, Guestrin C, XGBoost: A scalable tree boosting system. Proc. 22nd ACM SIGKDD Int. Conf. Know. Disc. Data Mining, 2016:785–794, arxiv.org/abs/1603.02754v3
[16] Grabczewski K, Meta-learning in decision tree induction, Studies in Computational Intelligence 498, 10.1007/978-3-319-00960-5_2.
[17] Bingham E, Kaski S, Laaksonen J, Lampinen L, Advances in independent component analysis and learning machines, Elsevier, Academic press, 2015, 10.1016/B978-0-12-802806-3.09987-5
[18] Pajunen P, Girolami M, Implementing decisions in binary decision trees using independent component analysis, Proceeding ICA, 2000:477-481.
[19] Quinlan JR, Simplifying decision trees, International Journal of Man-Machine Studies, 1987;27:221-234, http://hdl.handle.net/1721.1/6453.
[20] https://github.com/mdabros/SharpLearning (n.d.).